WILEY | Hindawi

Research Article

Speed Tracking and Synchronization of a Multimotor System Based on Fuzzy ADRC and Enhanced Adjacent Coupling Scheme

Liang Tao (ID)**, Qiang Chen** (ID)**, Yurong Nan** (ID)**, Fang Dong, and Yan Jin** (ID)

College of Information Engineering, Zhejiang University of Technology, Hangzhou Zhejiang 310023, China

Correspondence should be addressed to Yurong Nan; nyr@zjut.edu.cn

In this paper, a speed tracking and synchronization control approach is proposed for a multimotor system based on fuzzy active disturbance rejection control (FADRC) and enhanced adjacent coupling scheme. By employing fuzzy logic rules to adjust the coefficients of the extended state observer (ESO), FADRC is presented to guarantee the speed tracking performance and enhance the system robustness against external disturbance and parametric variations. Moreover, an enhanced adjacent coupling synchronization control strategy is proposed to simplify the structure of the speed synchronization controller through introducing coupling coefficients into the conventional adjacent coupling approach. Based on the proposed synchronization control scheme, an adaptive integral sliding mode control (AISMC) is investigated such that the chattering problem in conventional sliding mode control can be weakened by designing an adaptive estimation law of the control gain. Comparative simulations are carried out to prove the superiorities of the proposed method.

1. Introduction

The demands of control systems with large inertia and high power load are increasing in modern engineering systems [1]. However, due to the limited output torque, single-motor drive often fails to meet the control performance requirements when driving large inertia load and further affects the production efficiency. Recently, research on multimotor synchronous drive systems provides an effective way to solve the problem of large inertia load control and multimotor synchronous control has been applied in many manufactures [2]. However, there is a mutual coupling between motors in the multimotor system, which makes it difficult to ensure the system's trajectory tracking and synchronous control accuracy at the same time. Therefore, a superior speed synchronization control design is significant to achieve better synchronization performance of multimotor systems [3].

Some effective synchronous control strategies have been investigated in recent decades, such as master-slave synchronization strategy [4], adjacent coupling control [5], ring coupling synchronization technique [6], cross-coupling

synchronization strategy [7, 8], virtual line-shaft synchronization scheme [9], and relative coupling synchronization method [10]. Among all the above mentioned synchronization schemes, adjacent coupling control is designed based on minimum relative axial thought, which means that the torque of each motor should be able to make the tracking error of itself converge to zero and lead the synchronization error to converge to zero stably between any motor and adjacent motors. An adjacent cross coupling strategy combining with sliding mode control [5] is designed for a multiple induction motor synchronization control system. The speed tracking error and synchronize error are both guaranteed to converge to zero by Lyapunov stability theory. A total sliding mode control method based on adjacent cross coupling structure in [11] is proposed for the multiple induction motors. The speed tracking of each motor is stabilized by synchronizing with other motors, such that the synchronized errors can be converged to zero. However, the two methods cannot solve the chattering problem in the controller. Compared with other synchronization approaches, the adjacent coupling control has better synchronization performance with respect to faster convergence rate and smaller

steady-state error. However, there is an obvious disadvantage which is that conventional adjacent coupling control has a complex structure and difficult stability proof [12]. An enhanced adjacent coupling synchronization method with coupling coefficients is developed in this paper so that the controller structure is simplified and stability is proved more easily.

To further improve the tracking control performance, various modern control algorithms combined with aforementioned synchronization schemes are investigated and have acquired good results. Reference [13] combined an adaptive sliding mode technique with a ring coupling scheme to achieve rapid and accurate tracking and synchronization performance. Reference [14] designed a master-slave consensus tracking algorithm via observer for coordination control of multimotor systems, which could guarantee the synchronization precision. Reference [15] constructed a synchronization controller using a fuzzy neural network to deal with the nonlinear problem effectively. Reference [16], investigated a fast terminal sliding mode synchronization scheme of a dual-motor driving system, which accelerated the convergence rates of tracking error and synchronization error. Moreover, more advanced control methods are also employed for multimotor systems, such as H_∞ control [17], fuzzy control [18], and integral terminal sliding mode [19].

Compared to other control methods, active disturbance rejection control (ADRC) is a new-fashioned application algorithm and has acquired wide application in various fields, such as aerospace and vehicle manufacture [20–23]. There are some excellent merits of ADRC including error-based character, strong robustness for external disturbance and parametric variations, and superior response rate [24–28]. A nonlinear ADRC [24] is investigated for induction motors to guarantee the robust control and high performance by employing the ESO to observe the derivative signals and precise decoupling of the motor without accurate prior knowledge. An enhanced linear ADRC [25] is designed for an interior permanent magnet synchronous motor on the basis of a HF pulse voltage signal injection scheme. The cascaded ESO is proposed to ensure the timely and accurate estimation of the lumped disturbance. A novel control scheme is proposed for ball screw feed drives in [26] to improve the tracking performance and robustness of the system by combining ADRC and the proportional integral method. The ESO is employed to estimate and compensate the unmodeled dynamics, disturbances, and cutting load. However, as one of the most important parts in ADRC, the parameters of ESO mentioned in above literatures are chosen in advance, which may restrict its flexibility and cause poor dynamic system performance [29].

Since the parameters of ESO directly affect the observation of disturbances and uncertainties and then affect the control performance of ADRC, the optimization design of the parameters of ESO has been studied. An ant colony optimization (ACO) algorithm [30] is investigated to optimize the six parameters of ESO for an induction motor system by the self-learning ability of ACO. Thus, the robustness of the proposed optimization scheme is better than traditional ADRC when perturbation is produced. An adaptive hybrid biogeography-based optimization and differential evolution (AHBBODE) is represented in [31] for vessels with a dynamic positioning system to achieve the accurate movement and positioning. AHBBODE is employed to optimize the parameters of ADRC, which are not easily obtained by the trial and error method. A new Levy fight-based whale optimization algorithm [32] is proposed to estimate the parameters of ADRC for an automatic carrier landing system with internal dynamics and external disturbance. The accurate tracking performance and robustness are obtained by using the proposed optimization algorithm. However, the optimizations of [30–32] are all offline optimization algorithms and the implements are more complex. When the system is suddenly influenced by the external environment, the control of offline parameter identification may not fully guarantee the system performance. The neural network observer is designed in [33] to estimate the unmeasurable system state variables, and the weight parameter is adaptive updating online. But the weight parameter is not easy to converge to the optimal value by traditional adaptive technique [34]. Among the numerous parameter optimization methods, the fuzzy logic is a powerful tool in parameter adjustment because of its simple structure, online optimization, and easy implementation [35], and thus, it is possible to use the optimization method based on fuzzy logic to adjust the ESO parameters, so as to further improve the system control performance.

Besides, for the purpose of keeping high synchronization control performance of a multimotor system, the lumped disturbances including nonlinearities and uncertainties should be compensated. In practical multimotor applications, the lumped disturbances always follow the operation of the system, which may arise internally, such as friction and parametric variations, or externally, such as change of the load. Among the numerous feedback control schemes, the sliding mode control (SMC) technique is a superior approach which can guarantee an efficient antidisturbance performance [36–41]. A total SMC is proposed to achieve speed tracking and synchronization for multimotor induction by employing adjacent cross coupling structure in [37]. Reference [38] designed an observer-based sliding mode controller for stochastic systems. By designing the observer and a product of sliding mode variable and negative definite matrix, the sliding mode variable can be stabled almost in the beginning and the sliding mode motion can be confirmed. Reference [39] managed to attenuate chattering based on a composite controller which is set by the sliding mode feedback and disturbance compensation with a new second-order model for the speed loop.

Motivated by the discussions mentioned above, the main contributions of this paper are summarized as follows:

(1) A fuzzy active disturbance rejection control (FADRC) is developed for multimotor systems to guarantee tracking performance and enhance the system robustness. Since the ESO parameters are

optimized by using fuzzy logic rules, the proposed FADRC can achieve a faster response than ADRC.

(2) By introducing coupling coefficients into adjacent coupling approach, an improved adjacent coupling scheme is proposed so that the controller structure is simplified and stability is proved more easily. Moreover, an AISMC approach is developed and incorporated into the synchronization control scheme to attenuate the chattering phenomenon in SMC.

The rest of this paper is organized as follows. The mathematical model of the multimotor system and the adjacent coupling scheme are shown in Section 2. In Section 3, two control schemes including a FADRC and an AISMC using improved adjacent coupling are designed for the multimotor system. The stability analysis is given in Section 4. Simulations are presented in Section 5, and a concise conclusion is provided in Section 6.

2. Problem Formulation

2.1. Mathematical Model of the Single-Motor System. The mathematical model of a surface-mounted permanent magnet synchronous motor (PMSM) under the d-q axis can be described as

$$
\begin{aligned}
u_d &= Ri_d + \dot{\psi}_d(t) - \omega \psi_q, \\
u_q &= Ri_q + \dot{\psi}_q(t) - \omega \psi_d, \\
\psi_d &= \psi_f + L_d i_d, \\
\psi_q &= L_q i_q,
\end{aligned}
\tag{1}
$$

where u_d, u_q are the stator voltages of d-axis and q-axis, respectively; i_d, i_q denote the stator currents of d-axis and q-axis; $\psi_d(t)$, $\psi_q(t)$ are the stator flux linkages of d-axis and q-axis; L_d, L_q are the inductances of d-axis and q-axis; ψ_f is the rotor flux linkage; ω is the angular speed of the the motor. It can be easily concluded that the model is strongly coupled between i_d and i_q according to (1) and $i_d = 0$ is often used to achieve decoupling for i_d and i_q. The control schematic diagram of each PMSM in a multimotor control system is given in Figure 1.

The electromagnetic torque of PMSM can be represented as

$$
T_e = 1.5m\left[\psi_d i_q - \psi_q i_d\right] = 1.5m\left[\psi_f i_q + \left(L_d - L_q\right) i_d i_q\right],
\tag{2}
$$

where m is the number of motor pole pairs. As a surface-mounted PMSM is employed, the permeability of permanent magnets and air permeability are almost the same. Hence, it is reasonable to think that $L_d - L_q = 0$. Thus, (2) is written as

$$
T_e = 1.5m\psi_f i_q.
\tag{3}
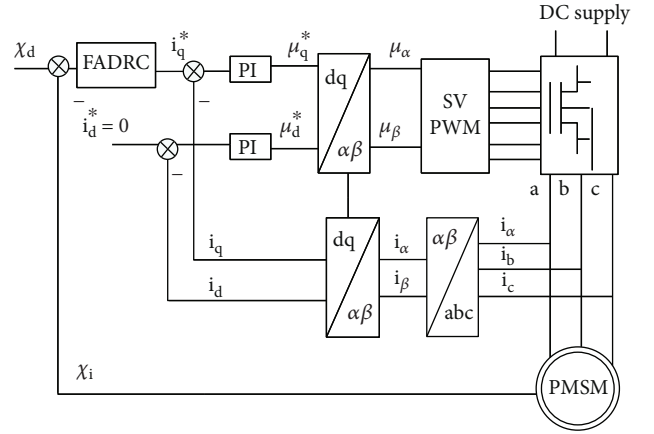$$

The motion dynamics of PMSM can be shown as

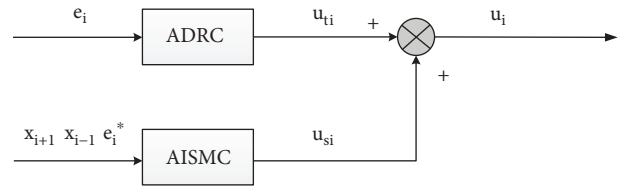FIGURE 1: The control schematic diagram of each PMSM.

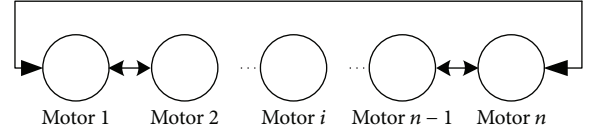FIGURE 2: Block diagram of the controller for each motor.

FIGURE 3: Simplified structure of synchronization control.

$$
J\dot{\omega}(t) = T_e - T_L - b\omega(t),
\tag{4}
$$

where J denotes the rotary inertia; T_L and b represent the load torque and viscous coefficient of friction, respectively. Due to the great influences of load torque, it is regarded as an external system disturbance.

Substituting (3) into (4), the following equation is obtained:

$$
\dot{\omega}(t) = \frac{1.5m\psi_f}{J} i_q - \frac{b}{J}\omega(t) - \frac{1}{J}T_L.
\tag{5}
$$

2.2. Mathematical Model of the Multimotor System. The mathematical model of the multimotor system is

$$
\dot{\omega}_i(t) = \frac{1.5m\psi_{f,i}}{J_i} i_{q,i} - \frac{b_i}{J_i}\omega_i(t) - \frac{1}{J_i}T_L,
\tag{6}
$$

where $\omega_i(t)$, $i = 1, \ldots, n$, represents the angular speed of the ith motor and n denotes the motor number.

In order to facilitate the controller design, defining equivalent variables $x_i(t) = \omega_i(t)$, $A_i = 1.5m\psi_{f,i}/J_i$, $B_i = -b_i/J_i$, $C_i = -1/J_i$, and $i_{q,i} = u_i$. Then (6) can be rewritten as
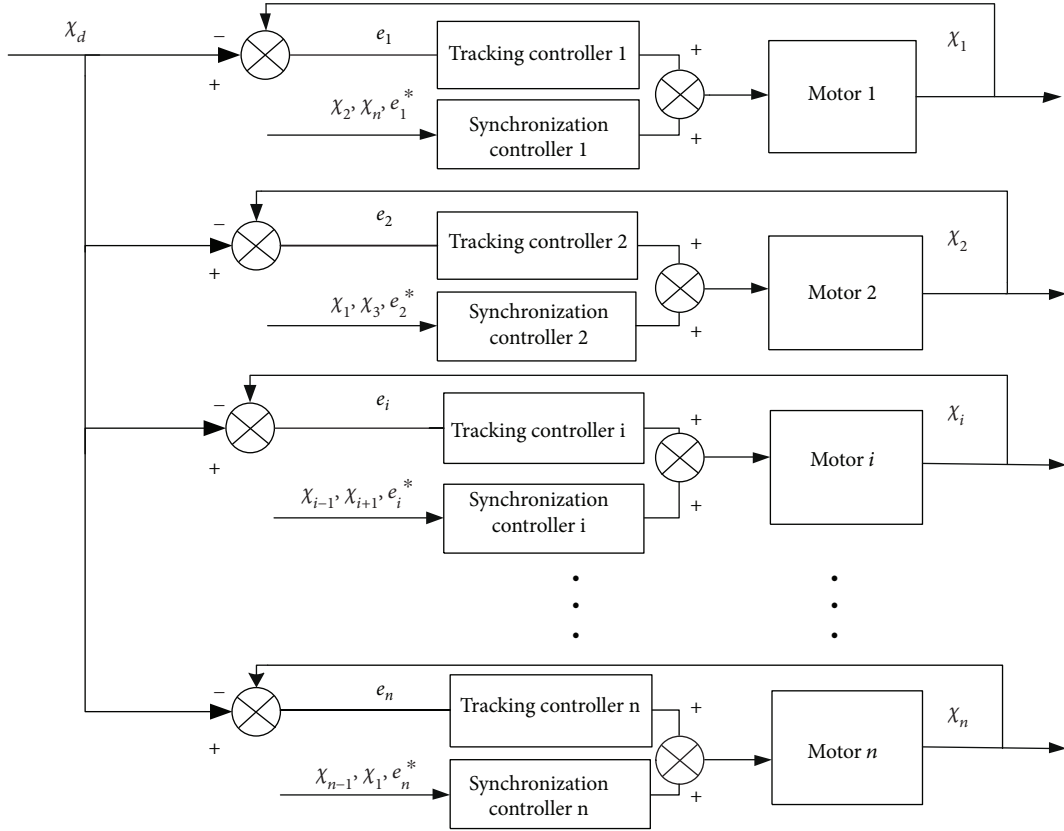
FIGURE 4: Schematic diagram of enhanced adjacent coupling.

$$\dot{x}_i(t) = A_i u_i + B_i x_i + C_i T_L. \qquad (7)$$

Considering the external disturbance and parameter variations, (7) can be transformed into

$$\dot{x}_i(t) = A_i u_i + B_i x_i + D_i, \qquad (8)$$

where D_i denotes the sum of external disturbance and parameter variations, which satisfies the boundness condition that $|D_i| \leq \Upsilon$, and Υ is the upper bound. The expression of D_i is

$$D_i = \Delta A_i u_i + \Delta B_i x_i + (C_i + \Delta C_i) T_L, \qquad (9)$$

where ΔA_i, ΔB_i, and ΔC_i denote the parameter variations.

2.3. Adjacent Coupling Scheme. The speed tracking error of the conventional adjacent coupling scheme can be defined as follows:

$$e_i(t) = x_d - x_i, \qquad (10)$$

where x_d represents the identical speed reference signal of each motor for the multimotor system.

The speed synchronization errors of adjacent motors are defined as

$$\varepsilon_1(t) = e_1(t) - e_2(t),$$
$$\vdots$$
$$\varepsilon_i(t) = e_i(t) - e_{i+1}(t), \qquad (11)$$
$$\vdots$$
$$\varepsilon_n(t) = e_n(t) - e_1(t).$$

In general, the larger synchronization errors will be generated at the initial stage of the system or when the external disturbances are encountered. Once $\varepsilon_i(t) \to 0$, all the motors have achieved a good synchronization performance.

For the purpose of keeping good synchronization performance for the multimotor system, the adjacent coupling errors are defined for the conventional adjacent-coupling synchronization technique

$$e_1^{\varepsilon}(t) = \varepsilon_1(t) - \varepsilon_n(t),$$
$$\vdots$$
$$e_i^{\varepsilon}(t) = \varepsilon_i(t) - \varepsilon_{i-1}(t), \qquad (12)$$
$$\vdots$$
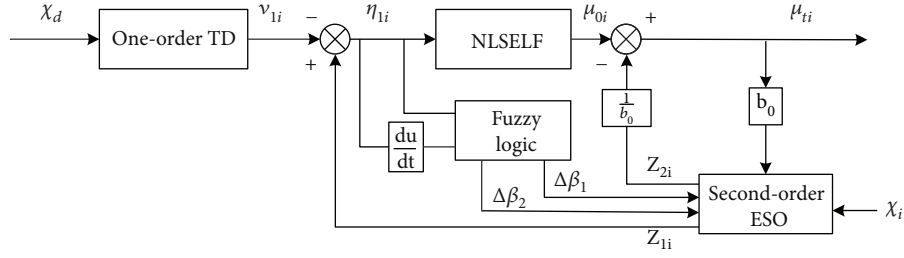$$e_n^{\varepsilon}(t) = \varepsilon_n(t) - \varepsilon_{n-1}(t).$$

Figure 5: Schematic diagram of FADRC.

It should be noted that in order to enhance the synchronization performance of the multimotor control system, both synchronization error and adjacent coupling error should be considered simultaneously in the controller design. However, the approach may greatly increase the complexity of controller and lead to the difficulty of the system stability analysis.

In this paper, the control objective is to design the speed tracking and synchronization controllers for the multimotor system such that

(1) the rotor speeds of all the motors can track the command speed signal, that is, $e_i \rightarrow 0$, $i = 1, \ldots, n$;

(2) each motor can synchronize other motors, that is, $\varepsilon_i \rightarrow 0$, $i = 1, \ldots, n$.

3. Controller Design

In this section, two controllers are proposed for the speed tracking and synchronous control of the multimotor system based on ADRC and AISMC, respectively. The design objectives of speed tracking and synchronization controllers are to ensure that the speed tracking errors and synchronization errors, respectively, can effectively converge to zero. The block diagram of the controller for each motor is given in Figure 2.

3.1. Enhanced Adjacent Coupling Scheme. An enhanced adjacent coupling scheme is developed for the multimotor system (total number of motors is n) to reduce the synchronization errors between the adjacent motors. The speed signal of each motor and adjacent motor are used as the input of the controller. Simultaneously, coupling coefficients are added to ensure that the synchronization errors converge to zero and simplify the design of the synchronous controller. The simplified structure of synchronization control is given in Figure 3, and Figure 4 shows the control schematic diagram of the enhanced adjacent coupling scheme.

In the enhanced adjacent coupling synchronization scheme, coupling coefficients are introduced into adjacent coupling errors to ensure the stability of the multimotor system and simplify the controller design. Consequently, the adjacent coupling errors are defined as

$$e_1^*(t) = p\varepsilon_1(t) - q\varepsilon_n(t),$$
$$\vdots$$
$$e_i^*(t) = p\varepsilon_i(t) - q\varepsilon_{i-1}(t), \tag{13}$$
$$\vdots$$
$$e_n^*(t) = p\varepsilon_n(t) - q\varepsilon_{n-1}(t),$$

where $p > 0$ and $q > 0$ and satisfying $p^n \neq q^n$.

Let

$$E = A * \varepsilon, \tag{14}$$

where

$$A = \begin{bmatrix} p & 0 & \cdots & \cdots & 0 & -q \\ \vdots & \ddots & & & 0 & \\ 0 & -q & p & \cdots & \cdots & \vdots \\ \vdots & \cdots & -q & p & \vdots & \vdots \\ \vdots & & & \vdots & \ddots & 0 \\ 0 & \cdots & \cdots & 0 & -q & p \end{bmatrix},$$

$$\varepsilon = \begin{bmatrix} \varepsilon_1(t) \\ \vdots \\ \varepsilon_i(t) \\ \vdots \\ \varepsilon_n(t) \end{bmatrix},$$

$$E = \begin{bmatrix} e_1^*(t) \\ \vdots \\ e_i^*(t) \\ \vdots \\ e_n^*(t) \end{bmatrix}. \tag{15}$$

The above matrix A can be transformed into the following triangular form by a reasonable equivalent transformation

$$
A = \begin{bmatrix} p & 0 & \cdots & \cdots & 0 & -q \\ \vdots & \ddots & & & & \vdots \\ 0 & \cdots & p & \cdots & \cdots & \vdots \\ 0 & \cdots & 0 & p & & -\dfrac{q^i}{p^{i-1}} \\ \vdots & & & \vdots & \ddots & \vdots \\ 0 & \cdots & & 0 & 0 & p - \dfrac{q^n}{p^{n-1}} \end{bmatrix}. \tag{16}
$$

It can be obtained that (14) has a unique solution when A is a full-rank matrix, that is, $p^n \neq q^n$. Once that condition E converges to a minimal domain is satisfied, then ε converges to a minimal domain, which means that the synchronization control objective can be transformed to design the speed synchronization controller to ensure that E converges to a minimal domain.

3.2. Speed Tracking Controller. ADRC is a powerful antidisturbance technique, including tracking differentiator (TD), ESO, and nonlinear state error feedback (NLSEF) controller. Smoother input signals and smaller overshoot can be obtained by using TD when the system starts. And the multimotor states and lumped disturbances including nonlinearities and uncertainties can be effectively observed by designing the ESO. The NLSEF is employed to realize lumped disturbance compensation with the feedback state errors. Figure 5 shows the detailed schematic diagram of FADRC.

From (7), the ith motor's tracking FADRC is designed as (17), (18), (19), and (20).

Firstly, the TD is given as

$$
\begin{aligned}
\eta_{0i} &= v_{1i} - x_d, \\
\dot{v}_{1i} &= -r \mathrm{fal}(\eta_0, \alpha, \delta),
\end{aligned} \tag{17}
$$

where v_{1i} denotes the output of TD, which indicates the tracking of the identical speed reference signal x_d; η_{0i} represents the error between v_{1i} and x_d; $a > 0, \delta > 0$ are the tuning parameters; $\mathrm{fal}(.)$ indicates a nonlinear function and is expressed as

$$
\mathrm{fal}(\eta, \alpha, \delta) = \begin{cases} \dfrac{\eta}{\delta^{1-\alpha}}, & |\eta| \leq \delta, \\ |\eta|^{\alpha} \operatorname{sign}(\eta), & |\eta| > \delta. \end{cases} \tag{18}
$$

Secondly, the ESO is designed as

$$
\begin{aligned}
\eta_i &= z_{1i} - x_i, \\
\dot{z}_{1i} &= z_{2i} - \beta_1 \mathrm{fal}(\eta, a, \delta) + A_i u_{ti} + B_i z_{1i}, \\
\dot{z}_{2i} &= -\beta_2 \mathrm{fal}(\eta, a, \delta),
\end{aligned} \tag{19}
$$

TABLE 1: Fuzzy rules of $\Delta \beta_i$ $(i = 1, 2)$.

e_{01}	e_{02}				
	PB	PS	ZO	NB	NS
PB	PB/NB	PS/NS	PS/NS	ZO/ZO	PS/NS
PS	PB/NS	PS/NS	PS/NS	NS/PS	ZO/ZO
ZO	PS/NS	PS/NS	ZO/ZO	NS/PS	NS/PS
NB	ZO/ZO	NS/PS	NS/PS	NB/PB	NS/PS
NS	PS/NS	ZO/ZO	NS/PS	NB/PS	NS/PS

where z_{1i} is the observation value of x_i and $z_{2i} = D_i$ is the lumped disturbance; η_i is the observation error of x_i; $\beta_1 > 0$ and $\beta_2 > 0$ are the tuning gains.

Remark 1. According to (18), the nonlinear function $\mathrm{fal}(.)$ will produce a larger gain when observation error η_i is small; on the contrary, $\mathrm{fal}(.)$ will produce a smaller gain when η_i is large. Reference [40] pointed out that $\mathrm{fal}(.)$ could stabilize the observation state by choosing the appropriate size of β_i $(i = 1, 2)$, which means that $|x_i - z_{1i}| \leq d_1, |D_i - z_{2i}| \leq d_2$, where d_1 and d_2 are all small positive constants.

Finally, the NLSEF is designed as

$$
\begin{aligned}
\eta_{1i} &= v_{1i} - z_{1i}, \\
u_{0i} &= \beta_3 \mathrm{fal}(\eta_{1i}, a, \delta), \\
u_{ti} &= u_{0i} - \dfrac{z_{2i}}{b_0},
\end{aligned} \tag{20}
$$

where u_{0i} and u_{ti} indicate the control input without considering disturbance and speed tracking control signal with considering disturbance, respectively, of the ith motor; η_{1i} denotes the error between the output v_{1i} of TD and the output z_{1i} of ESO; $b_0 > 0$ is a constant, which represents the estimated value of A_i and is given by experience.

It is pointed out in [20] that a ADRC-based single-input and single-output system is absolutely stable, and thus, the speed tracking errors are ensured to converge to zero through the speed tracking controller.

3.3. Coefficient Determination via Fuzzy Logic Rules. In the following, we define that

$$
\begin{aligned}
e_{01} &= \eta_i, \\
e_{02} &= \dot{\eta}_i.
\end{aligned} \tag{21}
$$

In practical applications, the coefficients of ESO, β_i, $(i = 1, 2)$, are usually adjusted based on prior knowledge to acquire a good estimation performance. However, it may restrict its flexibility and cause poor dynamic system performance. In the following, the error variables e_{01} and e_{02} are utilized by the fuzzy logic rules to determine the coefficients β_i, which can be optimally adjusted online.

The error variables e_{01} and e_{02} are employed as the fuzzy inputs, and five linguistic rules, that is, positive big (PB),

positive small (PS), zero (ZO), negative big (NB), and negative small (NS), are given as the membership functions. Table 1 shows the fuzzy rules of $\Delta\beta_i$. And a Gaussian function and a triangle function are chosen as the input e_{01}, e_{02} membership function and the output $\Delta\beta_i$ ($i = 1, 2$) membership function, respectively. In this subsection, the basic universe of e_{01} and the basic universe of e_{02} are $[-1, +1]$ and $[-0.5, +0.5]$, and $\Delta\beta_i$ are chosen within $[-0.1, +0.1]$ and $[-0.5, +0.5]$, respectively. The Mamdani type is adopted as the fuzzy inference, and the weighted average method is utilized for the defuzzification.

According to Table 1 and after fuzzy inference and defuzzification, the coefficient β_i is rectified as

$$\beta_1 = \beta_1' + \Delta\beta_1,$$
$$\beta_2 = \beta_2' + \Delta\beta_2, \tag{22}$$

where β_i' and $\Delta\beta_i$ are the initial value and rectified value, respectively, of the ESO coefficients.

3.4. Speed Synchronization Controller.
In this subsection, we employ AISMC to design the speed synchronization controller.

The integral sliding mode surface can be designed as

$$S_i(t) = e_i^* + \lambda \int_0^t e_i^*(\tau)d\tau, \tag{23}$$

where $\lambda > 0$ denotes a tuning parameter. From (8) and (23), the general sliding mode surface controller based on ESO is given as

$$u_{si}' = \frac{1}{A_i}\left[-z_{2i} + B_i x_i + \frac{p}{p+q}\dot{x}_{i+1} + \frac{q}{p+q}\dot{x}_{i-1} + \frac{\lambda}{(p+q)}e_{i+1}^* - l_i \operatorname{sign}(S_i)\right], \tag{24}$$

where l_i is the control gain that satisfies that $l_i \geq d_2 \geq 0$. The state variables can be stabilized to the sliding surface by the designing of controller (24).

However, it is difficult to determine the accurate value of l_i since the upper bounds of estimation errors are not easy to obtain. Therefore, in the following, an AISMC combined with ESO is designed as

$$u_{si} = \frac{1}{A_i}\left[-z_{2i} - B_i x_i + \frac{p}{p+q}\dot{x}_{i+1} + \frac{q}{p+q}\dot{x}_{i-1} + \frac{\lambda}{(p+q)}e_i^* - \widehat{l}_i \operatorname{sign}(S_i)\right], \tag{25}$$

where the adaptive law of $\widehat{l}_i$ is

$$\dot{\widehat{l}}_i = \begin{cases} \sigma_m |S_i| \operatorname{sign}(|S_i| - \varepsilon), & \widehat{l}_i > \sigma, \\ \sigma, & \widehat{l}_i \leq \sigma, \end{cases} \tag{26}$$

where $\sigma_m > 0$ and $\sigma > 0$ are used to guarantee that $\widehat{l}_i > 0$.

Substituting (25) into (8), we have

$$\dot{x}_i(t) = -z_{2i} + \frac{p}{p+q}\dot{x}_{i+1} + \frac{q}{p+q}\dot{x}_{i-1} + \frac{\lambda}{(p+q)}e_i^* - \widehat{l}_i \operatorname{sign}(S_i) + D_i. \tag{27}$$

4. Stability Analysis

Lemma 1 (see [42]). *For the given nonlinear uncertainty system (8) with the sliding mode (23), the control gain $\widehat{l}_i(t)$ has an upper bound, which satisfies that $\widehat{l}_i(t) \leq l_i$.*

Lemma 2 (see [43]). *Suppose that there is a continuous and positive definite function $V(t)$, which satisfies the follow differential equation:*

$$\dot{V}(t) \leq -\alpha_0 V^\xi, \quad V(t_0 > 0), \tag{28}$$

where $\alpha_0 > 0$ and $0 < \xi < 1$ are positive constants. Then for any given t_0, there is a finite time t_1 that satisfies

$$V^{1-\xi}(t) \leq V^{1-\xi}(t_0) - \alpha_0(1-\xi)(t-t_0), \quad t_0 \leq t \leq t_1,$$
$$V(t) \equiv 0, \quad \forall t \geq t_1, \tag{29}$$

where $t_1 = t_0 + (V^{1-\xi}(t_0)/\alpha_0(1-\xi))$.

Theorem 1. *Considering multimotor system (8), integral sliding mode surface (23), and controller (25), the integral sliding mode surface S_i can converge to be uniformly ultimately bounded in finite time and the synchronization error can stably converge to be uniformly ultimately bounded when $\rho \leq \sigma_m \varepsilon/(k_\alpha + \varepsilon)$ with ϵ and k_α being two positive constants.*

Proof 1. Considering system (8), the Lyapunov function is designed

$$V_i = \frac{1}{2}S_i^2 + \frac{1}{2\rho}\tilde{l}_i^2, \tag{30}$$

where $\tilde{l}_i = \widehat{l}_i - l_i$.

Differentiating (30) and substituting into (13), we can obtain

$$\dot{V}_i = S_i * \dot{S}_i + \frac{1}{\rho}\tilde{l}_i\dot{\tilde{l}}_i = S_i(\dot{e}_i^*(t) + \lambda e_i^*(t)) + \frac{1}{\rho}\tilde{l}_i\dot{\tilde{l}}_i$$
$$= S_i[p(\dot{e}_i(t) - \dot{e}_{i+1}(t)) - q(\dot{e}_{i-1}(t) - \dot{e}_i(t)) + \lambda e_i^*] + \frac{1}{\rho}\tilde{l}_i\dot{\tilde{l}}_i. \tag{31}$$

Substituting (10) into (31), we have

TABLE 2: Parameters of four motors.

Parameter	Motor 1	Motor 2	Motor 3	Motor 4
$R_S(\Omega)$	2.875	2.875	2.88	2.86
$L_d(H)$	0.0085	0.0085	0.0085	0.0085
$L_q(H)$	0.0085	0.0085	0.0085	0.0085
$\psi_f(Wb)$	0.067	0.072	0.076	0.068
$J(kg{\bullet}m^2)$	0.008	0.0083	0.0073	0.0065
$B(N{\bullet}m{\bullet}s)$	0.00051	0.00047	0.00056	0.00061
$m(kg)$	1	1	1	1

$$
\dot{V}_i = S_i \left[p\dot{x}_{i+1}(t) - p\dot{x}(t)_i + q\dot{x}_{i-1}(t) - q\dot{x}_i(t) + \lambda e_i^* \right]
$$
$$
+ \frac{1}{\rho} \tilde{l}_i \dot{\tilde{l}}_i = S_i[p\dot{x}_{i+1}(t) - (p+q)\dot{x}_i(t) + q\dot{x}_{i-1}(t) + \lambda e_i^*] + \frac{1}{\rho}\tilde{l}_i\dot{\tilde{l}}_i.
$$
(32)

Substituting (27) into (32), then

$$
\dot{V}_i = S_i[-z_{2i} - l\,\text{sign}\,(S_i) + D_i(t)] + \frac{1}{\rho}\left(\hat{l}_i - l_i\right)\dot{\hat{l}}_i
$$
$$
= S_i\left[(D_i(t) - z_{2i}) - \hat{l}_i\,\text{sign}\,(S_i)\right]
$$
$$
+ \frac{1}{\rho}\left(\hat{l}_i - l_i\right)\dot{\hat{l}}_i \le |S_i||D_i(t) - z_{2i}| - \hat{l}_i|S_i|
$$
$$
+ l_i|S_i| - l_i|S_i| + \frac{1}{\rho}\left(\hat{l}_i - l_i\right)\dot{\hat{l}}_i \le -[l_i - d_2]|S_i|
$$
$$
- \left(\hat{l}_i - l_i\right)|S_i| + \frac{1}{\rho}\left(\hat{l}_i - l_i\right)\dot{\hat{l}}_i = -[l_i - d_2]|S_i|
$$
$$
+ \left(\hat{l}_i - l_i\right)\left(\frac{1}{\rho}\dot{\hat{l}}_i - |S_i|\right).
$$
(33)

Introducing parameter $k_a > 0$, (33) can be equivalently transformed into

$$
\dot{V}_i = -[l_i - d_2]|S_i| - \left(\hat{l}_i - l_i\right)\left(|S_i| - \frac{1}{\rho}\dot{\hat{l}}_i\right)
$$
$$
+ k_a\left|\hat{l}_i - l_i\right| - k_a\left|\hat{l}_i - l_i\right|.
$$
(34)

According to Lemma 1, we can obtain

$$
\dot{V}_i \le k_b|S_i| - \varrho - k_a\left|\hat{l}_i - l_i\right|,
$$
(35)

where $k_b = l_i - d_2 > 0$, $\varrho = ((1/\rho)\dot{\hat{l}}_i - |S_i|) - k_a)|\hat{l}_i - l_i|$. Ultimately, the derivative of V_i is

$$
\dot{V}_i \le k_b|S_i| - \varrho - k_a\left|\hat{l}_i - l_i\right|
$$
$$
= -\sqrt{2}k_b\frac{|S_i|}{\sqrt{2}} - \sqrt{2\rho}k_a\frac{\left|\hat{l}_i - l_i\right|}{\sqrt{2\rho}} - \varrho
$$
$$
\le -k_m V^{1/2} - \varrho,
$$
(36)

where $k_m = \min\{\sqrt{2}k_b, \sqrt{2\rho}k_a\}$.

Case 1. If $|S(i)| > \epsilon$, then according to (26), we have

$$
\dot{\hat{l}}_i = \sigma_m|S(i)|, \varrho = \left(\frac{1}{\rho}\sigma_m|S(i)| - |S(i)| - k_a\right)\left|\hat{l}_i - l_i\right|.
$$
(37)

When the parameter ρ is selected to satisfy $\rho \le \sigma_m\varepsilon/(k_\alpha + \varepsilon)$, we can conclude from (37) that $\varrho > 0$, which leads to $\dot{V}_i \le -k_m V_i^{1/2}$ from (36).

Case 2. Supposing that $|S(i)| \le \epsilon$, we have the function ϱ in (35) which is negative and $\dot{\hat{l}}_i$ is also negative. So, $\hat{l}_i$ will decrease until less than d_2. From (33), we can conclude that $\dot{V}_i$ will be positive, which means that $|S_i|$ will increase until larger than ϵ. Therefore, the case becomes the same as Case 1, in which $\dot{V}_i \le -k_m V_i^{1/2}$ can be finally guaranteed by choosing the appropriate parameter ρ.

From Case 1 and Case 2, we have $\dot{V}_i \le -k_m V_i^{1/2}$. According to Lemma 2, the sliding surface S_i could be guaranteed to converge to the domain $|S_i| \le \epsilon$ in finite time. According to $\dot{V}_i \le -k_m V_i^{1/2}$, we have $|S_i||\dot{S}_i| \le (\sqrt{2}/2)|k_m||S_i|$ so $|\dot{S}_i| \le (\sqrt{2}/2)k_m$. Differentiating both sides of (23), we have $|\dot{e}_i^* + \lambda e_i^*| \le (\sqrt{2}/2)k_m$ and the solution is $|e_i^*| \le e^{-\lambda t} + \epsilon$, which means that e_i^* converges to domain $|e_i^*| \le (\sqrt{2}/2)k_m$ when $t \to +\infty$. According to (14), we can conclude that ε_i converges to be uniformly ultimately bounded. This completes the theorem proof.

From (20) and (25), the complete speed controller for the ith motor can be obtained as

$$
u_i = u_{ti} + u_{si} = u_{0i} - \frac{z_{2i}}{b_0} + \frac{B_i x_i + p\dot{x}_{i+1}/(p+q) + q\dot{x}_{i-1}/(p+q) + \lambda e_i^*/(p+q) - l_i\,\text{sign}\,(S_i)}{A}.
$$
(38)

(a) Synchronization performances of M1

(b) Synchronization performances of M2

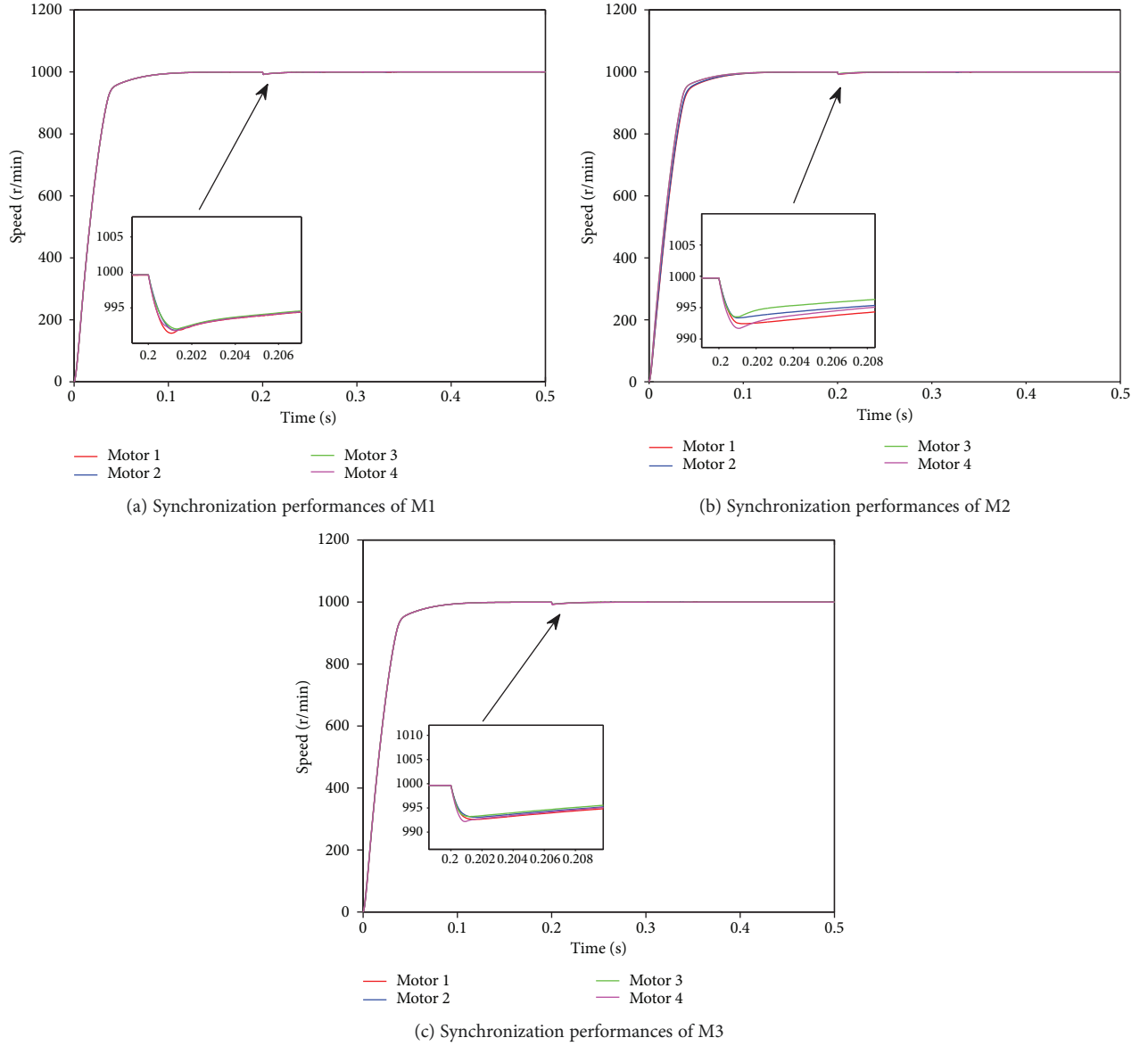(c) Synchronization performances of M3

FIGURE 6: Speed synchronization performance comparison.

Remark 2. To further improve the control performances, the function sign ($\bullet$), which may cause sliding mode chattering, is replaced by a saturation function sat($\bullet$)

$$\text{sat}(S_i) = \begin{cases} \dfrac{S_i}{\xi}, & |S_i| < \xi, \\ 1, & S_i \geq \xi, \\ -1, & S_i \leq -\xi, \end{cases} \tag{39}$$

where ξ is a small positive constant, which indicates the thickness of the boundary layer.

5. Simulation Results

In this section, numerical simulations are performed on a four-motor synchronization control system to evaluate the effectiveness of the proposed control scheme. In order to show the superior synchronization and tracking performance of the proposed method, two other different approaches and two different reference signals are provided for the fair comparison. For notation convenience, all the three methods are denoted as (M1) the proposed method, (M2) master-slave scheme with ADRC [44], and (M3) adjacent coupling scheme with SMC [12].

In the simulation, all the parameters of the four motors are shown in Table 2. The simulation time and step size are set as 0.5 s and 0.001 s, respectively. The load torque is given as 2 N and changes to 11.8 N at 0.2 s. The detailed parameters are set as follows.

5.1. M1: The Proposed Method. The parameters in tracking controllers (17), (18), and (19) are $a = 0.3$, $\delta = 0.5$, $b_0 = 50$, $\beta_1' = 5000$, $\beta_2' = 50000$, and $r = 2000$; the parameters in

(a) Synchronization errors $e_{1,2}$

(b) Synchronization errors $e_{2,3}$

(c) Synchronization errors $e_{3,4}$

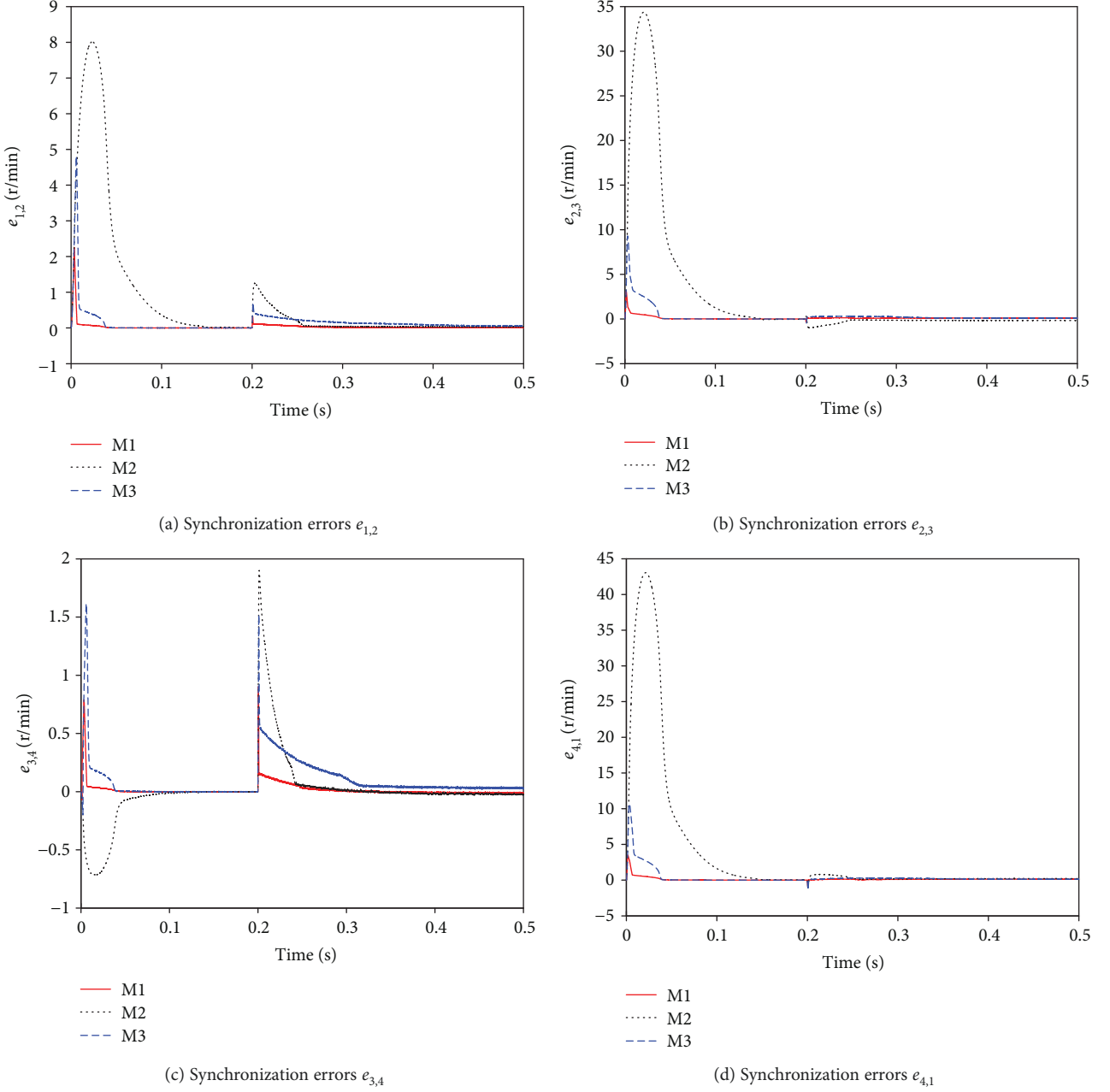(d) Synchronization errors $e_{4,1}$

FIGURE 7: Synchronization error comparison.

synchronization controller (25) are $p = 2$, $q = 1$, $\lambda = 30$, $l = 100$, and $\xi = 0.5$; the parameters of adaptive law (26) are set as $\sigma_m = 0.15$ and $\sigma = 0.01$.

5.2. M2: Master-Slave Scheme with ADRC.
The synchronization controller can be avoided to design for this method, because the command signals of other slave motors are the output signals of the master motor. The speed tracking controller has been shown in (20), and the relevant parameters are given as $a = 0.3$, $\delta = 0.5$, $b_0 = 50$, $\beta_1' = 5000$, $\beta_2' = 50000$, $\beta_3' = 500$, and $r = 2000$.

5.3. M3: Adjacent Coupling Scheme with SMC.
In this control approach, the speed tracking and synchronization controller are designed according to the procedures of [10], which can be expressed as follows, respectively.

$$u_{ti}^* = \frac{1}{A_i} [\dot{x}_d - B_i x_i + l_i \, \text{sign} \, (S_i) + \lambda e_i],$$

$$u_{si}^* = \frac{1}{A_i} \left[-B_i x_i + \frac{p}{p+q} \dot{x}_{i+1} + \frac{q}{p+q} \dot{x}_{i-1} + \frac{\lambda}{(p+q)} e_i^* - l_i \, \text{sign} \, (S_i) \right],$$
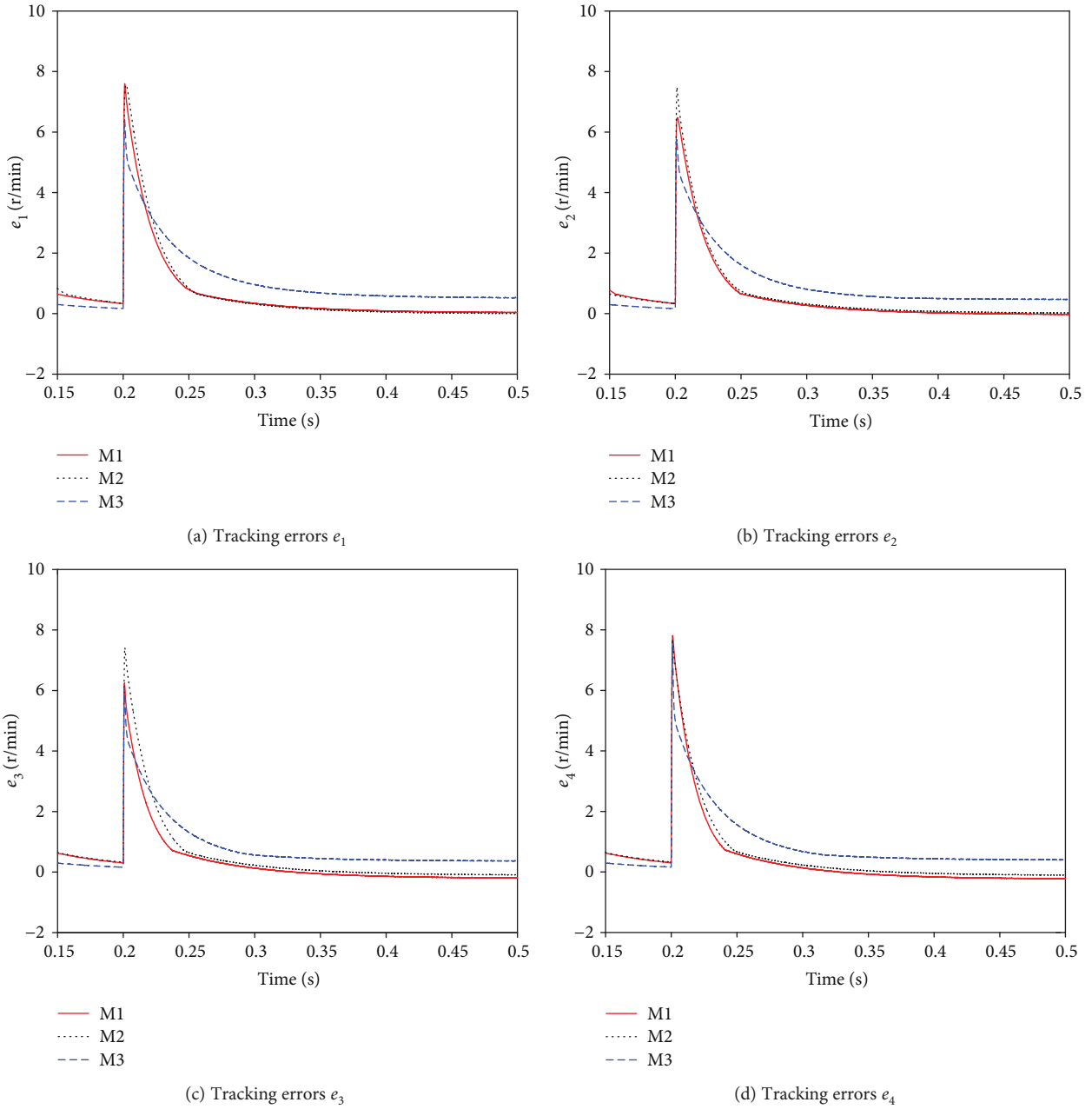
$$(40)$$

(a) Tracking errors e_1

(b) Tracking errors e_2

(c) Tracking errors e_3

(d) Tracking errors e_4

FIGURE 8: Tracking error comparison.

where $l_i = 500$, $i = 1, \ldots, 4$ and p, q, λ, A_i, B_i are set the same as M1.

In the following, two different command signals are given for comparison.

(1) $x_d = 1000$ r/min.

The speed synchronization performance comparison of four motors is shown in Figure 6. From Figure 6, we can see that the output speed signals of four motors with M1 can achieve the best synchronization performance when command signal is $x_d = 1000$ r/min. Moreover, M1 has a faster convergent speed than the other two methods when

motors suffer to load torque variations. The corresponding synchronization errors and tracking errors are shown in Figures 7 and 8, respectively. In Figure 7, $e_{i,j}$, $i, j = 1, \ldots, 4$ and $i \neq j$, indicates the synchronization error between the i*t h* motor and j*th* motor and we can see that the maximum synchronization error with M2 is about 40 r/min and the synchronization error with M3 is about 10 r/min. However, the maximum synchronization error with M1 is no more than 5 r/min. Consequently, we can conclude that compared with M2 and M3, M1 has a good performance with respect to small synchronization errors. As seen in Figure 8, it is clear to see that tracking error using M1
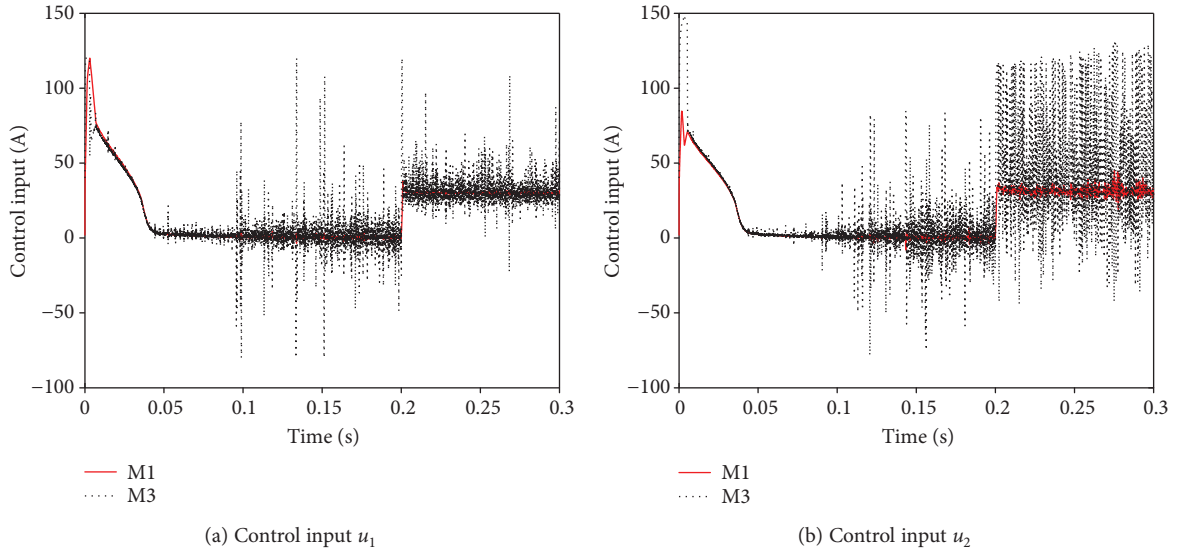
(a) Control input u_1

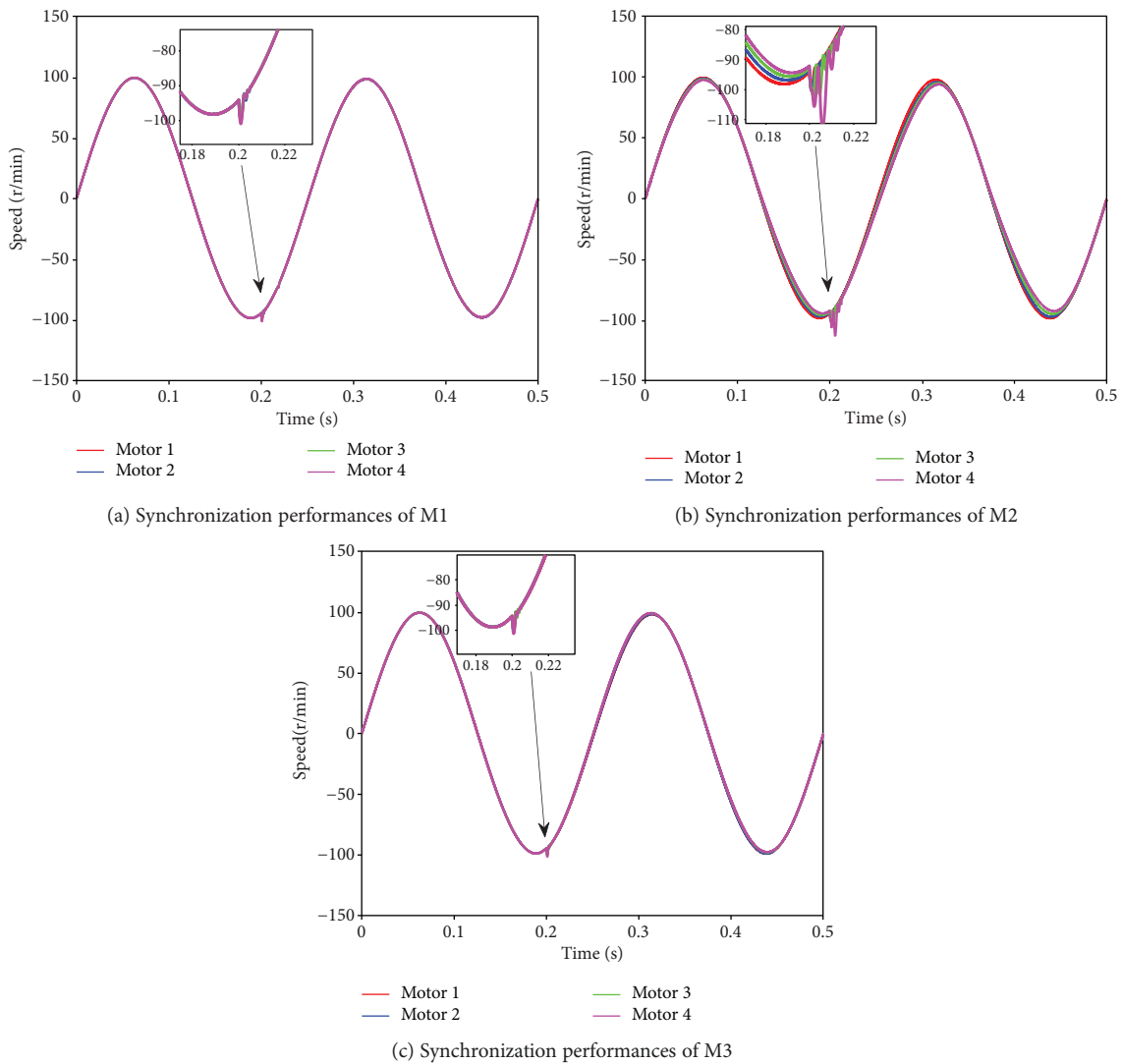(b) Control input u_2

FIGURE 9: Control inputs.

(a) Synchronization performances of M1

(b) Synchronization performances of M2

(c) Synchronization performances of M3

FIGURE 10: Speed synchronization and tracking performances.

(a) Synchronization errors $e_{1,2}$

(b) Synchronization errors $e_{2,3}$

(c) Synchronization errors $e_{3,4}$

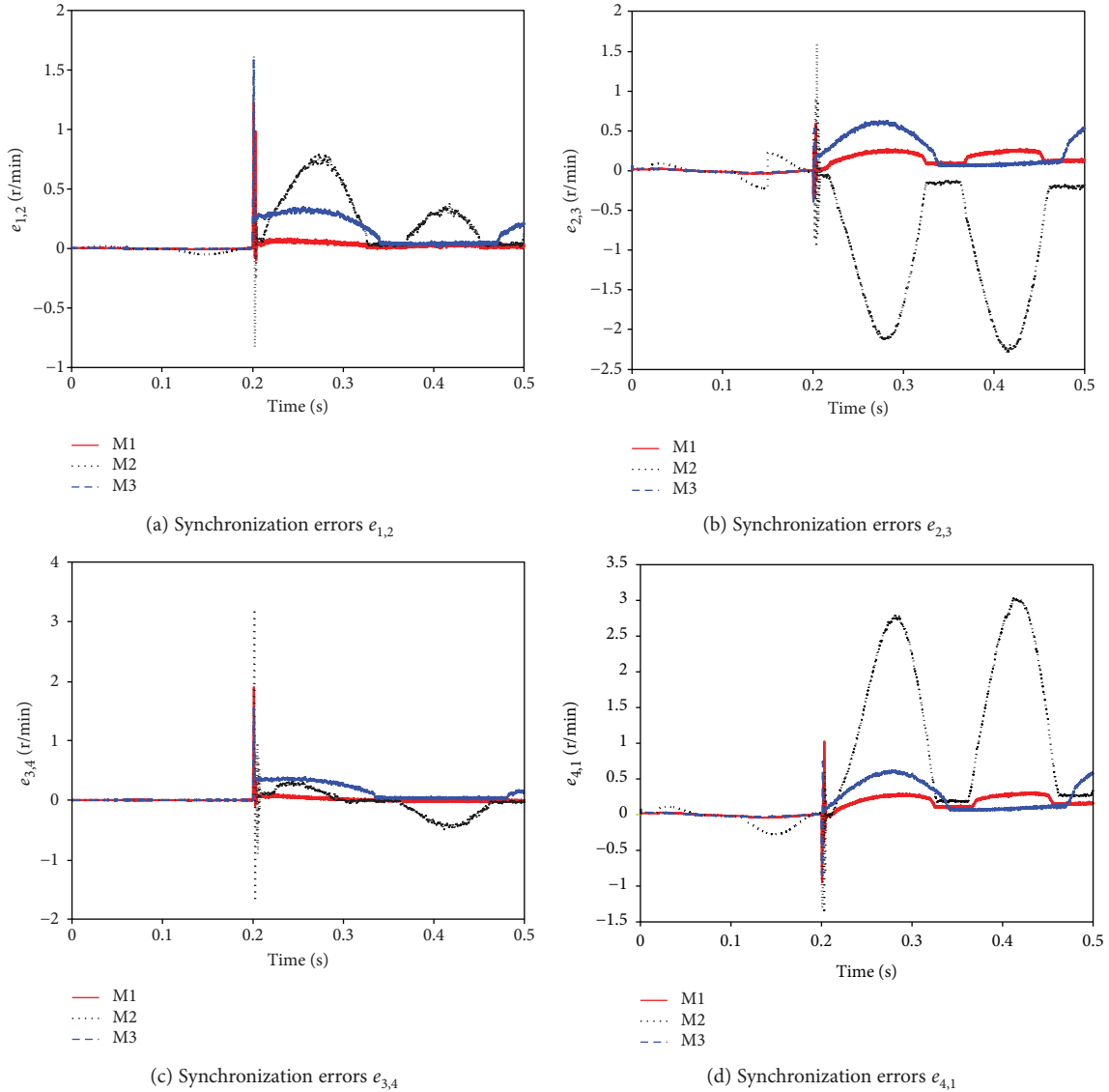(d) Synchronization errors $e_{4,1}$

FIGURE 11: Synchronization error comparison.

has a faster convergence rate when suffering to load variation. The control input signals with M1 and M3 are compared in Figure 9, which shows that the chattering problem with M1 is much smaller than M3.

(2) $x_d = 100\sin(8\pi t)$ r/min.

All the parameters are chosen the same as those in the former case. The speed synchronization performance comparison of four motors is shown in Figure 10. From Figure 10, we can see that speed synchronization performance with M1 is superior to that with the other two methods. The corresponding synchronization errors and tracking errors are provided in Figures 11 and 12, respectively. It is clear to see from Figure 11 that the synchronization errors of M1 have faster convergence rate and smaller steady-state values than those of M2 and M3. Figure 12 shows that M1 has smaller tracking errors compared to M2 and M3. The control input signals with M1 and M3 are

compared in Figure 13. From Figure 13, we can see that M1 can attenuate the chattering problem compared to M3, which verified the effectiveness of the proposed method.

From all the simulations above, we can conclude that

(1) Compared with M2, M1 has faster convergence rate when suffering to load variation;

(2) Compared with M3, M1 has a much smaller chattering problem;

(3) For different command signals, M1 can achieve better synchronization and tracking performance compared with M2 and M3.

6. Conclusion

Two kinds of controllers are investigated in this paper to improve the synchronization and tracking performances of
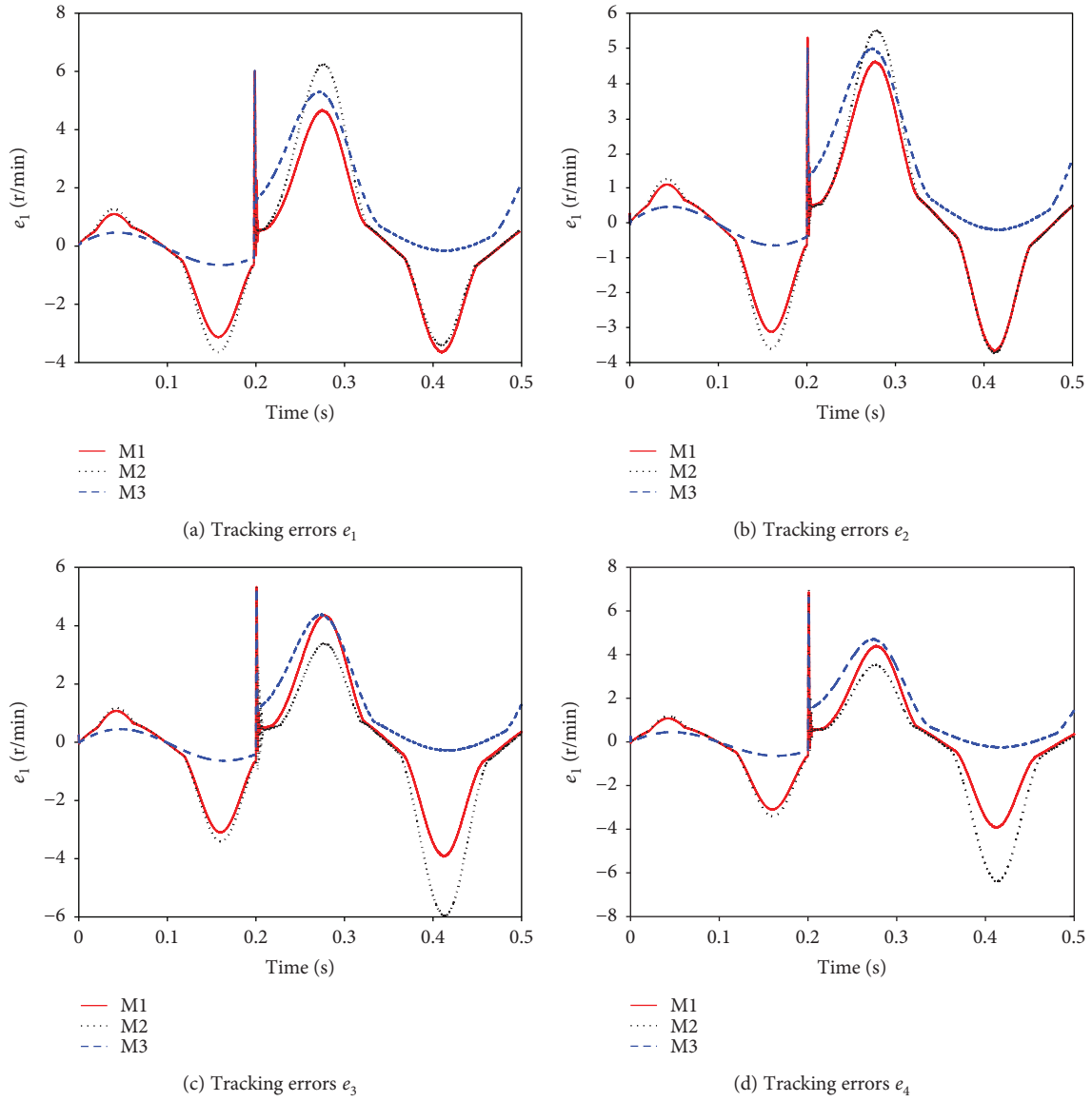
(a) Tracking errors e_1

(b) Tracking errors e_2

(c) Tracking errors e_3

(d) Tracking errors e_4

Figure 12: Tracking error comparison.
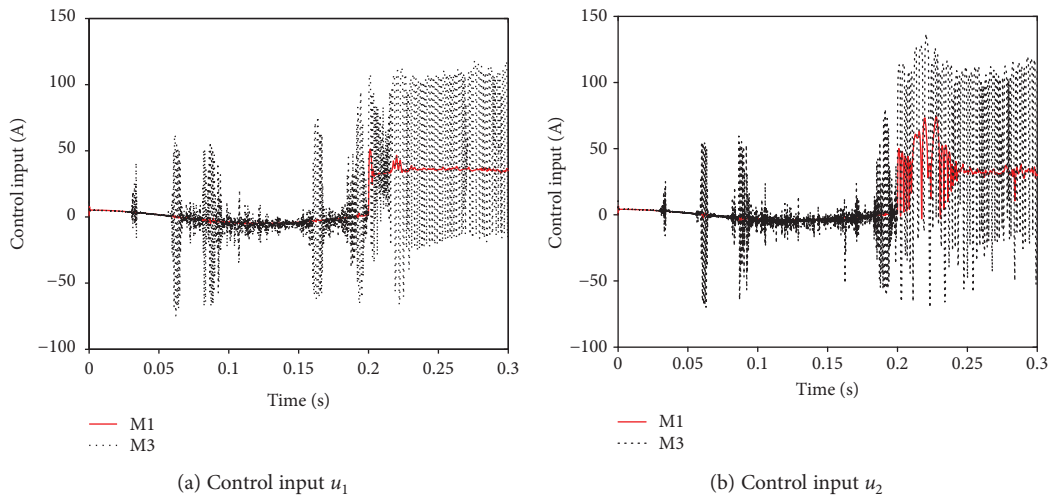

(a) Control input u_1

(b) Control input u_2

Figure 13: Control inputs.

the multimotor system. The synchronous controller is designed to ensure the speed synchronous performances and reduce the SMC chattering of the adjacent motor by utilizing an enhanced adjacent coupling approach with an adaptive integral sliding mode control. For the second tracking controller, the fuzzy logic rules are employed to design the active disturbance rejection control technique, and thus, a fast performance response and better robustness can be achieved. Simulation results prove the superior synchronization and tracking performance of the proposed method. The future work is aimed at simplifying the controller design and applying the proposed method to a practical system, such as a straight wire drawing machine.

Data Availability

The data used to support the findings of this study are available from the corresponding author upon request.

Conflicts of Interest

The authors declare that they have no conflicts of interest.

Acknowledgments

References

[1] S. Wang, J. Na, and X. Ren, "RISE-based asymptotic prescribed performance tracking control of nonlinear servo mechanisms," *IEEE Transactions on Systems, Man, and Cybernetics: Systems*, no. 99, pp. 1–12, 2017.

[2] Q. Chen, X. Ren, and J. Na, "Robust finite-time chaos synchronization of uncertain permanent magnet synchronous motors," *ISA Transactions*, vol. 58, pp. 262–269, 2015.

[3] M. Wang, X. Ren, Q. Chen, S. Wang, and X. Gao, "Modified dynamic surface approach with bias torque for multi-motor servomechanism," *Control Engineering Practice*, vol. 50, no. 4, pp. 57–68, 2016.

[4] F. J. Torres, G. V. Guerrero, C. D. Garcia, J. F. Gomez, M. Adam, and R. F. Escobar, "Master-slave synchronization of robot manipulators driven by induction motors," *IEEE Latin America Transactions*, vol. 14, no. 9, pp. 3986–3991, 2016.

[5] D. Z. Zhao, C. W. Li, and J. Ren, "Speed synchronisation of multiple induction motors with adjacent cross-coupling control," *IET Control Theory and Applications*, vol. 4, no. 1, pp. 119–128, 2010.

[6] R. Liu, J. Z. Sun, Y. Q. Luo, W. Sun, and W. D. Li, "Research on multi-motor synchronization control based on the ring coupling strategy for cutterhead driving system of shield machines," *Applied Mechanics and Materials*, vol. 52-54, pp. 65–72, 2011.

[7] G. Y. Zhao, B. Y. Zhuang, G. M. Zheng, and Y. G. Zhao, "Cross-coupling control method for five-axis computer numerical control machine with dual rotary tables," *Advances in Mechanical Engineering*, vol. 9, no. 9, Article ID 168781401773368, 2017.

[8] W. Chen, J. Liang, and T. Shi, "Speed synchronous control of multiple permanent magnet synchronous motors based on an improved cross-coupling structure," *Energies*, vol. 11, no. 2, p. 282, 2018.

[9] M. A. Valenzuela and R. D. Lorenz, "Electronic line-shafting control for paper machine drives," *IEEE Transactions on Industry Applications*, vol. 37, no. 1, pp. 158–164, 2001.

[10] T. Shi, H. Liu, Q. Geng, and C. Xia, "Improved relative coupling control structure for multi-motor speed synchronous driving system," *IET Electric Power Applications*, vol. 10, no. 6, pp. 451–457, 2016.

[11] D. Z. Zhao, C. W. Li, and J. Ren, "Speed synchronization of multiple induction motors with total sliding mode control," *Systems Engineering-Theory & Practice*, vol. 29, no. 10, pp. 110–117, 2009.

[12] C. F. Zhang, L. Wen, Y. Y. Xiao, and J. He, "Sliding mode variable structure-based multi-shaft synchronous control method and its application in printing press," in *2013 10th IEEE International Conference on Control and Automation (ICCA)*, pp. 1082–1086, Hangzhou, China, June 2013.

[13] L. B. Li, L. L. Sun, S. Z. Zhang, and Q. Q. Yang, "Speed tracking and synchronization of multiple motors using ring coupling control and adaptive sliding mode control," *ISA Transactions*, vol. 58, no. 1, pp. 635–649, 2015.

[14] C. Zhang, H. Wu, J. He, and C. Xu, "Consensus tracking for multi-motor system via observer based variable structure approach," *Journal of the Franklin Institute*, vol. 352, no. 8, pp. 3366–3377, 2015.

[15] C. H. Zhang, Q. S. Shi, and J. Cheng, "Design of fuzzy neural network controller for synchronization drive in multimotor systems," *Control and Desicion*, vol. 22, no. 1, pp. 30–33, 2007.

[16] W. Zhao and X. M. Ren, "The fast terminal sliding mode control of dual-motor driving servo systems with friction," *Journal of Harbin Institute of Technology*, vol. 46, no. 3, pp. 119–123, 2014.

[17] C. S. Chen and L. Y. Chen, "Robust cross-coupling synchronous control by shaping position commands in multiaxes system," *IEEE Transactions on Industrial Electronics*, vol. 59, no. 12, pp. 4761–4773, 2012.

[18] S. Jie, T. Peng, X. Yuan, J. Xiangjun, and R. Malekian, "An improved synchronous control strategy based on fuzzy controller for PMSM," *Elektronika ir Elektrotechnika*, vol. 20, no. 6, pp. 17–23, 2014.

[19] D. Chen, H. Du, and X. Jin, "Position tracking control for permanent magnet synchronous motor based on integral high-order terminal sliding mode control," in *2017 32nd Youth Academic Annual Conference of Chinese Association of Automation (YAC)*, pp. 234–239, Hefei, China, May 2017.

[20] J. Q. Han, "From PID technique to active disturbances rejection control technique," *Control Engineering of China*, vol. 9, no. 13, pp. 13–18, 2002.

[21] Q. Chen, F. Dong, L. Tao, and Y. R. Nan, "Multiple motors synchronization based on active disturbance rejection control with improved adjacent coupling," in *2016 35th Chinese Control Conference (CCC)*, pp. 4510–4516, Chengdu, China, July 2016.

[22] Y. Huang and W. Xue, "Active disturbance rejection control: methodology and theoretical analysis," *ISA Transactions*, vol. 53, no. 4, pp. 963–976, 2014.

[23] Z. Chu, Y. Sun, C. Wu, and N. Sepehri, "Active disturbance rejection control applied to automated steering for lane keeping in autonomous vehicles," *Control Engineering Practice*, vol. 74, pp. 13–21, 2018.

[24] G. Feng, Y. F. Liu, and L. Huang, "A new robust algorithm to improve the dynamic performance on the speed control of induction motor drive," *IEEE Transactions on Power Electronics*, vol. 19, no. 6, pp. 1614–1627, 2004.

[25] G. Wang, R. Liu, N. Zhao, D. Ding, and D. G. Xu, "Enhanced linear ADRC strategy for HF pulse voltage signal injection based sensorless IPMSM drives," *IEEE Transactions on Power Electronics*, pp. 1–12, 2018.

[26] C. Zhang and Y. Chen, "Tracking control of ball screw drives using ADRC and equivalent-error-model-based feedforward control," *IEEE Transactions on Industrial Electronics*, vol. 63, no. 12, pp. 7682–7692, 2016.

[27] S. Li and J. Li, "Output predictor-based active disturbance rejection control for a wind energy conversion system with PMSG," *IEEE Access*, vol. 5, no. 99, pp. 5205–5214, 2017.

[28] G. Zhang, G. Wang, B. Yuan, R. Liu, and D. Xu, "Active disturbance rejection control strategy for signal injection based sensorless IPMSM drives," *IEEE Transactions on Transportation Electrification*, vol. 4, no. 1, pp. 330–339, 2018.

[29] S. Wang, X. Ren, J. Na, and T. Zeng, "Extended-state-observer-based funnel control for nonlinear servomechanisms with prescribed tracking performance," *IEEE Transactions on Automation Science and Engineering*, vol. 14, no. 1, pp. 98–108, 2017.

[30] Z. Yin, C. Du, J. Liu, X. Sun, and Y. Zhong, "Research on autodisturbance-rejection control of induction motors based on an ant colony optimization algorithm," *IEEE Transactions on Industrial Electronics*, vol. 65, no. 4, pp. 3077–3094, 2018.

[31] D. Wu, F. Ren, L. Qiao, and W. Zhang, "Active disturbance rejection controller design for dynamically positioned vessels based on adaptive hybrid biogeography-based optimization and differential evolution," *ISA Transactions*, vol. 78, pp. 56–65, 2018.

[32] Y. Yu, H. Wang, N. Li, Z. Su, and J. Wu, "Automatic carrier landing system based on active disturbance rejection control with a novel parameters optimizer," *Aerospace Science and Technology*, vol. 69, pp. 149–160, 2017.

[33] X. Liu, C. Yang, Z. Chen, M. Wang, and C.-Y. Su, "Neuro-adaptive observer based control of flexible joint robot," *Neurocomputing*, vol. 275, pp. 73–82, 2018.

[34] Y. Lv, J. Na, Q. Yang, X. Wu, and Y. Guo, "Online adaptive optimal control for continuous-time nonlinear systems with completely unknown dynamics," *International Journal of Control*, vol. 89, no. 1, pp. 99–112, 2016.

[35] Q. Chen, Y.-R. Nan, H. H. Zheng, and X. M. Ren, "Full-order sliding mode control of uncertain chaos in a permanent magnet synchronous motor based on a fuzzy extended state observer," *Chinese Physics B*, vol. 24, no. 11, article 110504, 2015.

[36] J. Na, M. N. Mahyuddin, G. Herrmann, X. Ren, and P. Barber, "Robust adaptive finite-time parameter estimation and control for robotic systems," *International Journal of Robust and Nonlinear Control*, vol. 25, no. 16, pp. 3045–3071, 2015.

[37] C. W. Li, D. Z. Zhao, and J. Ren, "Total sliding model speed synchronization control of multi induction motors," *System Engineering-Theory & Practice*, vol. 29, no. 10, pp. 110–117, 2009.

[38] J. Li and Q. Zhang, "An integral sliding mode control approach to observer-based stabilization of stochastic Itô descriptor systems," *Neurocomputing*, vol. 173, no. 3, pp. 1330–1340, 2016.

[39] S. Li, K. Zong, and H. Liu, "A composite speed controller based on a second-order model of permanent magnet synchronous motor system," *Transactions of the Institute of Measurement and Control*, vol. 33, no. 5, pp. 522–541, 2011.

[40] J. Na, A. S. Chen, G. Herrmann, R. Burke, and C. Brace, "Vehicle engine torque estimation via unknown input observer and adaptive parameter estimation," *IEEE Transactions on Vehicular Technology*, vol. 67, no. 1, pp. 409–422, 2018.

[41] S. Mobayen, "Fast terminal sliding mode controller design for nonlinear second-order systems with time-varying uncertainties," *Complexity*, vol. 21, no. 2, 244 pages, 2015.

[42] F. Plestan, Y. Shtessel, V. Brégeault, and A. Poznyak, "Sliding mode control with gain adaptation—application to an electropneumatic actuator," *Control Engineering Practice*, vol. 21, no. 5, pp. 679–688, 2013.

[43] Q. Chen, L. Yu, and Y. Nan, "Finite-time tracking control for motor servo systems with unknown dead-zones," *Journal of Systems Science and Complexity*, vol. 26, no. 6, pp. 940–956, 2013.

[44] X. Q. Liu, J. Q. Hu, and L. Zhou, "Active disturbance rejection control of three-motor synchronous control system," *Proceedings of the CSEE*, vol. 30, no. 12, pp. 80–85, 2010.